nature geoscience

LETTERS

PUBLISHED ONLINE: 21 JUNE 2009 | DOI: 10.1038/NGEO550

The role of magma injection in localizing black-smoker activity

William S. D. Wilcock[1]*, Emilie E. E. Hooft[2], Douglas R. Toomey[2], Paul R. McGill[3], Andrew H. Barclay[1†], Debra S. Stakes[3†] and Tony M. Ramirez[3†]

Black-smoker hydrothermal systems at mid-ocean ridges are often driven by heat loss from a crustal magma chamber[1–3], but black-smoker systems have not been detected above all magma chambers[4,5]. The high fluxes of heat recorded at black-smoker systems require a thin, metre-scale conductive boundary layer at the top of the magma chamber, separating hydrothermal fluids from magma[2,6]. Extensive seismicity above the magma chambers[7–11] has been attributed to stresses from hydrothermal cooling[8–10,12]. The presence of high-temperature hydrothermal systems has previously been linked with episodes of magma chamber inflation[2,6,13,14], but the exact mechanism remained to be clarified. Here we analyse seismic data for the Endeavour segment of the Juan de Fuca ridge—a site of long-lived hydrothermal activity—recorded by seismometers located beneath the sea floor. Earthquake focal mechanisms derived from the data reveal a transition from normal faulting above the mid-crustal magma chamber to reverse faulting on either flank. This pattern of faulting is consistent with stress perturbations resulting from the emplacement of pressurized magma that forms a thin sill. We suggest that the ongoing recharge of magma into a crustal magma chamber not only replenishes the heat source[2,6,14], but also helps maintain a thin conductive boundary layer that would otherwise thicken owing to water–rock interactions and crystallization at the chamber roof.

The site of our study is the Endeavour segment of the Juan de Fuca ridge. The central portion of this segment hosts five high-temperature hydrothermal fields that are spaced 2–3 km apart along the ridge axis[15] (Fig. 1) and are driven by heat from an axial magma chamber (AMC) that is located 2.1–3.3 km below the sea floor[3]. The hydrothermal systems have been studied extensively since venting was discovered over two decades ago[15] and previous microearthquake experiments document high levels of associated seismicity[7,8]. In 1999, a magmatic intrusion accompanied by a large earthquake swarm perturbed the hydrothermal systems[16,17], leading to a reduction in gradients in fluid temperatures and chemistry across the Main Endeavour field[18] (Fig. 1). Otherwise, vigorous venting has persisted relatively unchanged for at least two decades[18,19].

The Keck seismic network (Fig. 1) was deployed in 2003 and comprised eight seismometers arrayed along a 10-km-long section of the ridge that includes the vent fields. Unlike previous microearthquake experiments, which used freefall ocean-bottom seismometers resting on the sea floor, all the seismometers were deployed below the sea floor by a remotely operated vehicle to ensure good coupling and minimize ocean-current-generated noise (details of the seismic instrumentation are provided in the Supplementary Methods).

Over the first year of operation, we located ~2,900 earthquakes within or near the network (Fig. 1a) with a minimum of five analyst picks and median 1σ location uncertainties of 0.3 km and 0.6 km in horizontal and vertical directions, respectively. Local magnitudes vary from 0.5 to 2.5, with a high b-value of 2.0 that is typical of earthquakes in volcanic and hydrothermal regions. The rate of on-axis seismicity and its spatial and magnitude distribution is broadly similar to that observed during earlier short-duration microearthquake experiments[7,8].

We combined precise relative arrival time picks obtained using cross-correlation with conventional analyst picks to relocate ~1,400 earthquakes using the double-difference technique[20], with each earthquake linked to at least one other with a minimum of eight analyst and four cross-correlated travel time differences. Estimated, 1σ relative location uncertainties for tightly grouped earthquakes within individual clusters can be as small as 10 m horizontally and 20 m vertically, whereas the relative location uncertainty between adjacent clusters is about five times this. Absolute 1σ uncertainties for earthquake clusters are several hundred metres.

Most of the earthquakes lie within a few-hundred-metre-thick region overlying or to the sides of the AMC, and most of the relocated earthquakes lie within tightly grouped clusters (Figs 1b and 2). There are clusters beneath the Mothra and Salty Dawg vent fields, and numerous clusters form an almost continuous arcuate band of earthquakes that follows the apparent curvature of the AMC from the High Rise vent field to south of the Main Endeavour. South of the Main Endeavour field, the earthquakes extend to shallower depths than elsewhere (Fig. 2). The presence of earthquakes on either side of the Main Endeavour field is consistent with the idea that chemical and thermal gradients across the field[18,19] are a result of two sources of upflow[15]. There is also a correlation between the density of earthquakes and the intensity of hydrothermal venting. Most of the earthquakes occur between the Main Endeavour and High Rise fields, which in comparison with the other vent fields on this segment are characterized by a larger number of black smoker vents[15], higher maximum venting temperatures[15] and higher heat fluxes, of several hundred megawatts[21].

We were able to determine well-constrained focal mechanisms for 170 earthquakes from P-wave first motions[22] (Fig. 3). Most of the focal mechanisms are for earthquakes between the Main

[1]University of Washington, School of Oceanography, Box 357940, Seattle, Washington 98195, USA, [2]University of Oregon, Department of Geological Sciences, Eugene, Oregon 97403, USA, [3]Monterey Bay Aquarium Research Institute, 7700 Sandholdt Road, Moss Landing, California 95039, USA.
[†]Present addresses: Lamont-Doherty Earth Observatory, 61 Route 9W, Palisades, New York 10964, USA (A.H.B.); Cuesta College, Division of Physical Sciences, San Luis Obispo, California 93403, USA (D.S.S.); Triton Imaging, 125 Westridge Drive, Watsonville, California 95076, USA (T.M.R.).
*e-mail: wilcock@u.washington.edu.

© 2009 Macmillan Publishers Limited. All rights reserved.

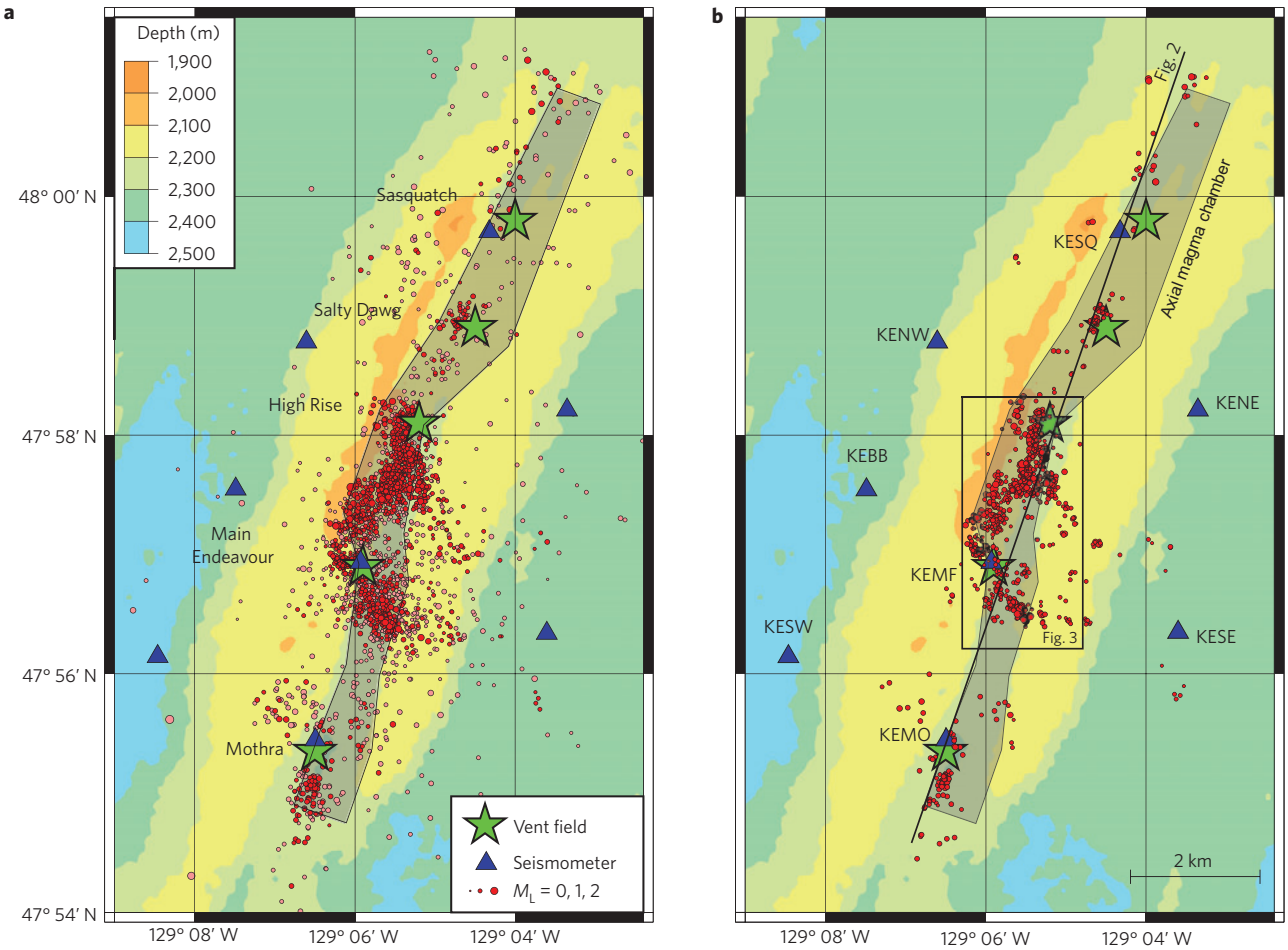

Figure 1 | Bathymetric maps showing the seismic network and earthquake epicentres. a, Epicentres for earthquakes obtained with Hypoinverse[31] (red and pink circles scaled by local magnitude, M_L, where red symbols distinguish the subset of earthquakes shown in **b**). The seismic network comprised eight seismometers (blue triangles). Also shown are the high-temperature vent fields (labelled green stars) and the approximate footprint of the AMC reflector at 2.3–3.1 km depth (grey shading)[3]. **b**, Epicentres for 1,444 earthquakes that were located with the double-difference algorithm HypoDD[20]. A solid black line shows the profile for the cross-section shown in Fig. 2 and a black box shows the area covered by Fig. 3. The seismic stations are labelled with their names.

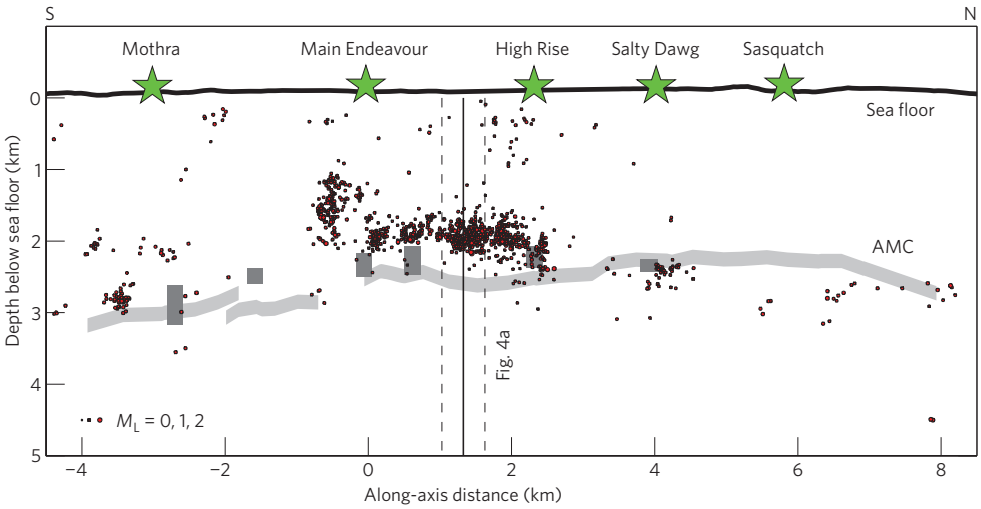

Figure 2 | Along-axis vertical cross-section showing hypocentres. Hypocentres for double-difference locations[20] lying within 1 km of the profile shown in Fig. 1b. Also shown are vent-field locations (green stars) and the position of the AMC reflector for along- (light-grey shading) and across-axis (dark-grey shading) multichannel reflection profiles[3]. A vertical black line shows the location of the across-axis cross-section of Fig. 4a, with dashed lines enclosing the earthquakes that are included on that section. The earthquakes beneath the Salty Dawg and Sasquatch vent fields that plot below the AMC have absolute location uncertainties consistent with locations above or to the side of the AMC.

© 2009 Macmillan Publishers Limited. All rights reserved.

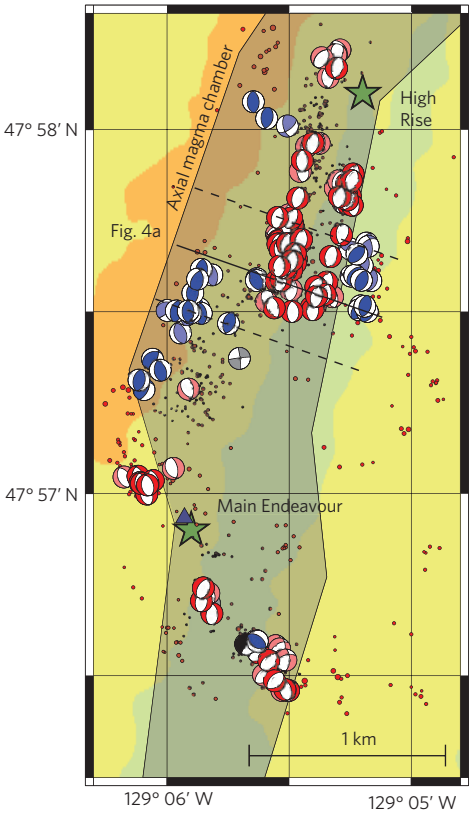

Figure 3 | Bathymetric map showing focal mechanisms. Detailed map of the region shown by a black box in Fig. 1b plotted using the same conventions with the addition of lower-hemisphere double-couple focal mechanisms determined from P-wave first motions[22]. Focal mechanisms are colour coded, with red for normal faulting, blue for thrust faulting and black for intermediate and strike-slip mechanisms. Lighter shading shows mechanisms with higher uncertainties. A solid black line and dashed lines to either side show the location and limits of earthquake projection for the cross-section shown in Fig. 4a. The bathymetry colour scale is the same as in Fig. 1—light green shading corresponds to the axial valley.

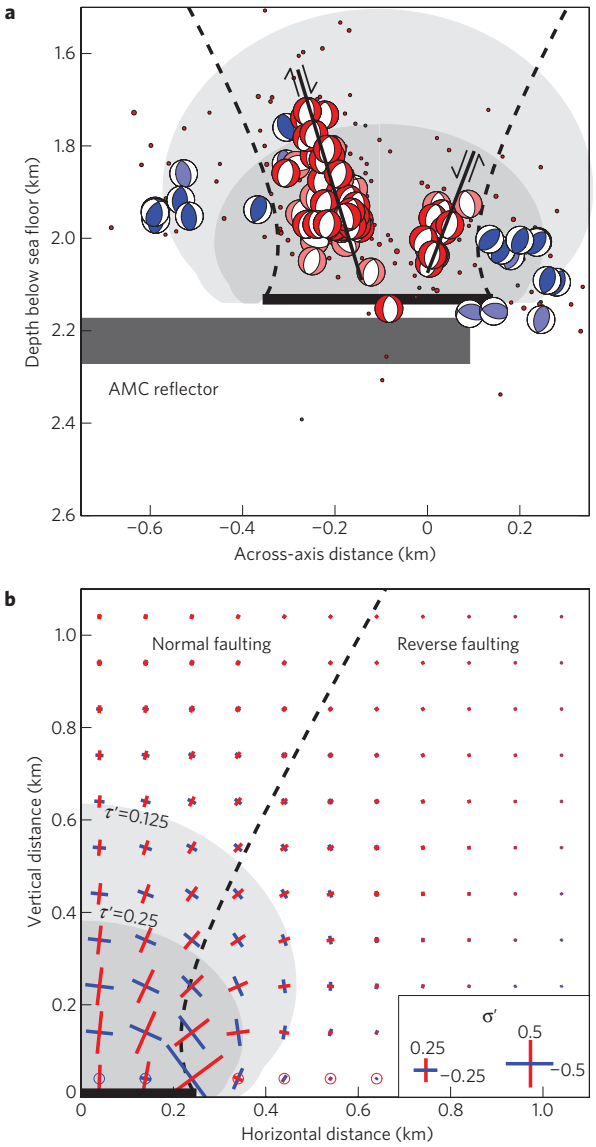

Figure 4 | Cross-section of the focal mechanisms and stress perturbations from a pressurized crack. a, Vertical cross-section along the profile in Fig. 3 showing hypocentres and focal mechanisms for earthquakes within 0.3 km of the profile. Also shown are the inferred normal faults (solid black lines), the position of the axial magma chamber (dark-grey shading) and the predicted stress perturbations above a pressurized crack plotted using the conventions of Fig. 4b. **b**, Stress perturbations above one side of a pressurized horizontal crack[25] of width 0.5 km (bold black line) showing maximum compressional and extensional normal stress perturbations, σ' (red and blue lines, respectively, with circles indicating stress maxima perpendicular to the section), and maximum shear stresses, τ' (shaded contours), all normalized to the overpressure in the crack. A dashed line shows the predicted transition from normal to reverse faulting on a ridge-parallel fault dipping at 45°.

Endeavour and High Rise fields that are confined to a 400-m-thick layer above the AMC (Fig. 4a). There are nearly 100 normal-faulting mechanisms in a region that extends ~1 km along the axis from just south of High Rise to midway between the fields. The hypocentres and focal mechanisms are consistent with two ridge-parallel normal faults that dip towards each other (Fig. 4a). This region of normal faulting is flanked to the east and southwest by groups of ~15 reverse-faulting mechanisms. On the west flank, most of the reverse-faulting earthquakes are offset to the south, but on the east flank the transition from normal to reverse faulting occurs in a ridge-perpendicular direction over no more than 100 m. Both reverse- and normal-faulting earthquakes occur throughout the deployment.

Normal-faulting earthquakes above the reaction zone have previously been interpreted in terms of thermal stresses from hydrothermal cooling[8–10]. In the simplest model, extensional earthquakes should be concentrated in the region of most intense cooling around a thin thermal boundary layer that would extend only a few metres away from the heat source[2,12]. This prediction is inconsistent with the observed vertical distribution of normal-faulting earthquakes. If adjacent volumes of rock are undergoing heating and cooling as a result of the upflow and downflow of cold and hot fluids, respectively, then thermal stresses could account for the observed focal mechanisms. However, we think this explanation is unlikely because it predicts variable fault strikes as the thermal stresses would be similar in all horizontal directions[8]. Furthermore, reverse-faulting mechanisms resulting from thermal expansion due to heating by hot rising fluids would be expected above the magmatic heat source rather than on both sides.

The earthquake mechanisms are better explained by the stress perturbations resulting from the injection of magma into a sill. The presence of two inward facing normal faults above the AMC is consistent with the formation of a graben over a region being extended by a magma intrusion[23], but this model does not explain

© 2009 Macmillan Publishers Limited. All rights reserved.

the presence of reverse faults on both sides of the normal faults. Seismic reflection data show that AMCs are thin horizontal or subhorizontal sills that typically extend ~1 km across axis with a vertical thickness of a few tens of metres[24]. If the AMC is modelled by a two-dimensional horizontal crack, the distribution of stresses induced by injecting overpressured magma[25] favours normal faulting above the crack and reverse faulting to either side, with the fault planes striking along axis (Fig. 4b). The predicted stress perturbations decrease over a characteristic vertical length scale of about half the crack width, and the region where significant stresses favour normal faulting is substantially larger than that favouring reverse faulting. Because magma overpressures would be relieved by any escape of volatiles, we envisage that ongoing magma injection is required to maintain the stress perturbations.

Our model has limitations. First, in most locations (Fig. 3) reverse faults are limited to one side of the ridge axis, which suggests either that the stress field has an asymmetric component that is not explained by the model or that the distribution of faults that are prone to failure is not uniform. Second, we do not account for the total stress field because background stresses are incompletely known and probably complex[26] and we know neither the absolute magma overpressure nor the Coulomb failure criteria for the small fault patches associated with the microearthquakes. Nevertheless, the simple model fits the data fairly well if the magma sill is ~0.5 km wide (Fig. 4b). This is smaller than the widths of 0.8–1.0 km reported from nearby multichannel seismic data, but the widths of reflection profiles are probably overestimated because of the presence of diffractions[24].

The analysis of multichannel reflection data from other locations shows that the composition of the AMC varies from pure melt to crystal mush and that hydrothermal vents seem to coincide with fully molten sections[13]. This observation led to the inference that enhanced hydrothermal activity is associated with recent magma supply[13]. At the Endeavour, we document strong evidence for ongoing magma injection beneath the two vent fields with highest maximum temperatures, heat fluxes and rates of seismicity. Geodetic observations from Axial volcano, another site of sustained high-temperature hydrothermal venting, also show that the volcano has been undergoing steady inflation since it erupted in 1998 (ref. 27). At 9° 50′ N on the East Pacific Rise, vigorous hydrothermal circulation persisted for 15 years between two eruptions[28], and it seems plausible that the magma chamber was re-inflating throughout this interval. On the basis of these observations we postulate that long-lived black smoker venting above mid-crustal magma chambers may coincide with the sites of ongoing magma recharge.

On the basis of the earthquake distribution and the style of faulting observed beneath the Endeavour vent field, we further suggest that seismogenic cracking associated with magma recharge provides a key mechanism that localizes high-temperature black-smoker vent fields. Long-term heat fluxes of hundreds of megawatts require a conductive boundary layer with a thickness of no more than a few metres[2,12]. If magma freezes onto the roof of the magma chamber[2,6] or water–rock reactions clog the deepest cracks[29], the conductive boundary layer will thicken. Models suggest that this former process will lead to a significant decline in heat fluxes and/or vent temperatures on timescales of about a year[2,6]. Furthermore, theoretical considerations also suggest that any thickening of the conductive boundary layer will lead to differential thermal stresses that put its upper portions into compression[30], inhibiting the growth of cracks and potentially further thickening the thermal boundary layer by closing existing cracks in the overlying rock. We argue that cracking induced by magma injection may provide a critical mechanism to counteract the processes that would otherwise thicken the thermal boundary layer and decrease heat fluxes.

Previous work has shown that the heat flux from black-smoker fields is compatible with reasonable estimates of magma recharge rates and has led to the inference that magma recharge may be a requirement for vigorous long-term hydrothermal circulation[2,6,14]. This interpretation can also explain why high-temperature vent sites are absent on some ridge sections that are underlain by an AMC (refs 4, 5) if they are not undergoing recharge. Furthermore, it suggests that knowledge of the global distribution and longevity of hydrothermal venting may provide direct constraints on spatial and temporal patterns of magma recharge to mid-crustal magma chambers.

Methods

Seismic analysis. Student analysts obtained preliminary phase picks and locations for 12,792 local and regional earthquakes recorded by the seismic network between 8 August 2003 and 1 August 2004. Earthquakes with epicentres within 3 km of the nearest station were repicked, and 2,862 proximal earthquakes with a minimum of five good-quality arrival time picks including at least one P and one S wave were relocated using the algorithm Hypoinverse[31]. Seismic moments and local magnitudes were calculated from the spectral amplitudes of P and S waveforms using standard methods[8].

We then cross-correlated P and S waves from each station to identify groups of arrivals with similar waveforms and picked the relative arrival times. We allowed for reversed polarities by aligning waveforms on the basis of the maximum magnitude of the cross-correlation coefficient. All correlated waveforms were inspected visually to eliminate suspect alignments and to pick P-wave first motions. We applied the double-difference algorithm HypoDD[20] to relocate 1,444 earthquakes, each of which is connected to at least one other earthquake with a minimum of eight analyst and four cross-correlated difference times. The relocation used 296,000 P-wave and 230,000 S-wave differential times from analyst picks and 55,000 P-wave and 61,000 S-wave differential times from cross-correlation. The root mean squared residuals for the differential travel times are 29 ms and 7 ms for analyst and cross-correlated times, respectively. Relative location uncertainties were estimated by relocating groups of ~50 earthquakes using singular value decomposition[20].

To obtain focal mechanisms we used the HASH algorithm[22], which uses multiple realizations of a grid search to find solutions that fit the polarity data given the uncertainties in the hypocentre. Of the 242 earthquakes with at least six unambiguous first motions, we obtained 105 solutions for which the r.m.s. difference between the acceptable fault planes and the preferred focal mechanism is less than 35°, and 65 more for which it is less than 45°. An expanded discussion of the seismic analysis methods is included in the Supplementary Information.

Stress-perturbation calculations. The stress perturbations above the magma lens were approximated using the analytical plane-strain solution for the stresses surrounding a thin pressurized two-dimensional crack, which are given by[25]

$$\sigma_{xx} = p\left(\frac{r}{(r_1 r_2)^{1/2}}\cos\left(\theta-\frac{\theta_1+\theta_2}{2}\right)-1-\frac{a^2 r}{(r_1 r_2)^{3/2}}\sin\theta\sin\frac{3(\theta_1+\theta_2)}{2}\right)$$

$$\sigma_{yy} = p\left(\frac{r}{(r_1 r_2)^{1/2}}\cos\left(\theta-\frac{\theta_1+\theta_2}{2}\right)-1+\frac{a^2 r}{(r_1 r_2)^{3/2}}\sin\theta\sin\frac{3(\theta_1+\theta_2)}{2}\right)$$

$$\sigma_{zz} = \nu\left(\sigma_{xx}+\sigma_{yy}\right)$$

$$\sigma_{xy} = p\frac{a^2 r}{(r_1 r_2)^{3/2}}\sin\theta\cos\frac{3(\theta_1+\theta_2)}{2}$$

$$\sigma_{xz} = \sigma_{yz} = 0$$

where σ is stress, subscripts x and y refer to directions parallel to and across the crack, respectively, z is the direction of invariance, p is the overpressure in the crack, r is the distance from the centre of the crack, r_1 and r_2 the distances to its two edges, θ the angular direction from the centre of the crack measured relative to the x axis, θ_1 and θ_2 the angular directions from the two crack edges, a the crack half-width and ν Poisson's ratio, which we take to be 0.245.

At each point on a 0.01 km grid, we compute the direction and magnitude of the principal stresses after removing the isotropic component from the solution. In Fig. 4b we plot vectors of the maximum compressional and extensional principal (normal) stresses on a 0.1 km grid and contours of the maximum resolved shear stresses. All stresses are normalized to the overpressure in the crack. We also plot the curve along which there is no resolved shear stress on a fault oriented at 45° relative to the crack. For a horizontal pressurized crack, this curve separates the regions where the stress perturbations favour normal and reverse faulting.

© 2009 Macmillan Publishers Limited. All rights reserved.

Received 16 December 2008; accepted 20 May 2009; published online 21 June 2009

References

1. Cann, J. R. & Strens, M. R. Black smokers fuelled by freezing magma. *Nature* **298**, 147–149 (1982).
2. Lowell, R. P. & Germanovich, L. N. On the temporal evolution of high-temperature hydrothermal systems at ocean ridge crests. *J. Geophys. Res.* **99**, 565–575 (1994).
3. Van Ark, E. M. *et al.* Seismic structure of the Endeavour Segment, Juan de Fuca Ridge: Correlations with seismicity and hydrothermal activity. *J. Geophys. Res.* **112**, B02401 (2007).
4. Haymon, R. M. *et al.* Hydrothermal vent distribution along the East Pacific Rise crest (9°09′–54′ N) and its relationship to magmatic and tectonic processes on fast-spreading mid-ocean ridges. *Earth Planet. Sci. Lett.* **102**, 513–534 (1991).
5. Hooft, E. E. E., Detrick, R. S. & Kent, G. M. Seismic structure and indicators of magma budget along the Southern East Pacific Rise. *J. Geophys. Res.* **102**, 27319–27340 (1997).
6. Liu, L. & Lowell, R. P. Models of hydrothermal heat output from a convecting, crystallizing, replenished magma chamber beneath an oceanic spreading centre. *J. Geophys. Res.* **114**, B02102 (2009).
7. McClain, J. S. *et al.* Seismicity and tremor in a submarine hydrothermal field: The northern Juan de Fuca Ridge. *Geophys. Res. Lett.* **20**, 1883–1886 (1993).
8. Wilcock, W. S. D., Archer, S. D. & Purdy, G. M. Microearthquakes on the Endeavour segment of the Juan de Fuca Ridge. *J. Geophys. Res.* **107**, 2336 (2002).
9. Sohn, R. A., Hildebrand, J. A. & Webb, S. C. A microearthquake survey of the high-temperature vent fields on the volcanically active East Pacific Rise. *J. Geophys. Res.* **104**, 25,367–25,377 (1999).
10. Sohn, R. A., Barclay, A. H. & Webb, S. C. Microearthquakes patterns following the 1998 eruption of Axial Volcano, Juan de Fuca Ridge: Mechanical relaxation and thermal strain. *J. Geophys. Res.* **109**, B01101 (2004).
11. Tolstoy, M. *et al.* Seismic identification of along-axis hydrothermal flow on the East Pacific Rise. *Nature* **451**, 181–185 (2008).
12. Lister, C. R. B. in *Hydrothermal Processes at Seafloor Spreading Centers* (eds Rona, P. A., Bostrom, K., Laubier, L. & Smith, K. L. Jr) 141–168 (Plenum, 1983).
13. Singh, S. C. *et al.* Seismic evidence for a hydrothermal layer above the solid roof of the axial magma chamber at the southern East Pacific Rise. *Geology* **27**, 219–222 (1999).
14. Humphris, S. E. & Cann, J. R. Constraints on the energy and chemical balances of the modern TAG and ancient Cyprus seafloor sulfide deposits. *J. Geophys. Res.* **105**, 28477–28488 (2000).
15. Kelley, D. S., Baross, J. A. & Delaney, J. R. Volcanoes, fluids, and life at mid-ocean ridge spreading centers. *Annu. Rev. Earth Planet. Sci.* **30**, 385–491 (2002).
16. Johnson, H. P. *et al.* Earthquake-induced changes in a hydrothermal system on the Juan de Fuca Ridge mid-ocean ridge. *Nature* **407**, 174–177 (2000).
17. Lilley, M. D., Butterfield, D. A., Lupton, J. E. & Olson, E. J. Magmatic events can produce rapid changes in hydrothermal vent chemistry. *Nature* **422**, 878–881 (2003).
18. Seyfried, W. E. Jr, Seewald, J. S., Berndt, M. E., Ding, K. & Foustoukos, D. I. Chemistry of hydrothermal vent fluids from the Main Endeavour Field, northern Juan de Fuca Ridge: Geochemical controls in the aftermath of the June 1999 seismic events. *J. Geophys. Res.* **108**, 2429 (2003).
19. Butterfield, D. A. *et al.* Gradients in the composition of hydrothermal fluids from the Endeavour segment vent field: Phase separation and brine loss. *J. Geophys. Res.* **99**, 9561–9583 (1994).
20. Waldhauser, F. HypoDD—a program to compute double-difference hypocenter locations *US Geol. Surv. Open File Rep.* 01-113 (2001).
21. Thompson, W. J. *et al.* Heat flux from the Endeavour segment of the Juan de Fuca Ridge. *Eos* **86**, Fall Meet. Suppl. abstr. T31A-0489 (2005).
22. Hardebeck, J. L. & Shearer, P. M. A new method for determining first-motion focal mechanisms. *Bull. Seismol. Soc. Am.* **92**, 2264–2276 (2002).
23. Rubin, A. M. Dike-induced faulting and graben subsidence in volcanic rift zones. *J. Geophys. Res.* **97**, 1839–1858 (1992).
24. Kent, G. M., Harding, A. J. & Orcutt, J. A. Evidence for a smaller magma chamber beneath the East Pacific Rise at 9°30′ N. *Nature* **344**, 650–653 (1990).
25. Pollard, D. D. & Segall, P. in *Fracture Mechanics of Rock* (ed. Atkinson, B. K.) 277–349 (Academic, 1987).
26. Buck, W. R., Einarsson, P. & Brandsdottir, B. Tectonic stress and magma chamber size as controls on dike propagation: Constraints from the 1975–1984 Krafla rifting episode. *J. Geophys. Res.* **111**, B12404 (2006).
27. Chadwick, W. W. Jr. *et al.* Vertical deformation monitoring at axial seamount since its 1998 eruption using deep-sea pressure sensors. *J. Volcanol. Geotherm. Res.* **150**, 313–327 (2006).
28. Tolstoy, M. *et al.* A sea-floor spreading event captured by seismometers. *Science* **314**, 1920–1922 (2006).
29. Wilcock, W. S. D. & Delaney, J. R. Mid-ocean ridge sulfide deposits: Evidence for heat extraction from magma chambers or cracking fronts? *Earth Planet. Sci. Lett.* **145**, 49–64 (1996).
30. Lister, C. R. B. Differential thermal stress in the Earth. *Geophys. J. R. Astron. Soc.* **86**, 319–330 (1986).
31. Klein, F. W. User's guide to HYPOINVERSE-2000, a Fortran program to solve for earthquake locations and magnitudes *US Geol. Surv. Open File Rep.* 02-171 (2002).

Acknowledgements

We thank J. Delaney and D. Kelley for their leadership of the programme that included this experiment; D. Bowman, J. Parker, H. Patel, C. Schmidt and student participants in a Friday Harbor Laboratories research apprenticeship for assistance with the initial data analysis and R. Lowell and R. Reves-Sohn for reviews that improved the manuscript. The W. M. Keck Foundation supported this research.

Author contributions

P.R.M., D.S.S. and T.M.R. developed and prepared the seismometers. All the authors participated in the experiment at sea. W.S.D.W., E.E.E.H., D.R.T. and A.H.B. oversaw the initial data analysis. W.S.D.W. completed the analysis and wrote the paper, with editing from the other authors.

Additional information

Supplementary information accompanies this paper on www.nature.com/naturegeoscience. Reprints and permissions information is available online at http://npg.nature.com/reprintsandpermissions. Correspondence and requests for materials should be addressed to W.S.D.W.

© 2009 Macmillan Publishers Limited. All rights reserved.